Applied Catalysis B: Environmental 150–151 (2014) 126–137

Contents lists available at ScienceDirect

Applied Catalysis B: Environmental

journal homepage: www.elsevier.com/locate/apcatb

In situ characterization of phase transformation and reactivity of high surface area lanthanum-based Ru catalysts for the combined reforming of methane

Betina M. Faroldi, John F. Múnera, Laura M. Cornaglia*

Instituto de Investigaciones en Catálisis y Petroquímica (FIQ, UNL- CONICET), Santiago del Estero 2829-3000, Santa Fe, Argentina

ARTICLE INFO

Article history:
Received 16 August 2013
Received in revised form
30 November 2013
Accepted 3 December 2013
Available online 12 December 2013

Keywords:
Combined reforming of methane
$La_2O_2CO_3$
Ruthenium
Hydrogen production
Pseudo in situ XPS and in situ LRS

ABSTRACT

A lanthanum oxycarbonate phase ($La_2O_2CO_3$) with high surface area was prepared as support of Ru catalysts. The metal was added by wet impregnation or incorporated during the oxycarbonate synthesis. The reactivity of the lanthanum and ruthenium species was studied through in situ Raman under dry reforming of methane conditions with and without oxygen addition. When Ru was incorporated by wet impregnation, the solid showed a higher reactivity of lanthanum oxycarbonate to the formation of La_2O_3 in a hydrogen flow even at low temperatures while RuO_x was completely reduced at 400 °C. It was also found that the reduced ruthenium species could be re-oxidized by CO_2 at the reaction temperature (550 °C). Under the dry reforming of methane, the metallic Ru did not change its oxidation state and the formation of graphitic carbon and oxycarbonate was observed. With the addition of oxygen, the same phase transformation occurred as in the case of the dry reforming of methane. However, the re-oxidation of Ru^0 species was observed through in situ Laser Raman spectroscopy and pseudo in situ XPS measurements. These measurements allowed us to advance in the understanding of the solid transformations produced during methane reforming reactions.

1. Introduction

The dry reforming of methane (DRM) has acquired importance in recent years as a means of obtaining high purity H_2. Natural gas production from hydrocarbon rich shale formations, known as "shale gas", is one of the most rapidly expanding trends in onshore oil and gas exploration and production today. Overall, unconventional natural gas is anticipated to become an ever-increasing portion of the proved reserves (extending over 100 years), while conventional gas reserves are declining [1].

With the goal of reducing energy consumption and increasing the production of hydrogen, it has been proposed to couple carbon dioxide reforming (endothermic) and partial oxidation (exothermic) of methane reactions. This process, which could be autothermal, confers significant added value to the reactions under study. In addition, hydrogen-permeable membrane reactors could improve the performance with respect to hydrogen in systems limited by thermodynamic equilibrium.

Lanthanum oxide shows interesting properties as promoter of highly dispersed metal catalysts and can modify the chemical behavior of some systems such as silica, ceria and alumina supports. It has been reported that the preparation procedure and composition strongly influences the microstructure of the promoter phase, the surface basicity and consequently the catalytic behavior [2–4]. It has also been reported that Ru catalysts [5] supported on commercial La_2O_3 have good activity and stability and present very low carbon deposition for the dry reforming of methane reaction. The high stability of these catalysts can be assigned to the metal support interaction. However, the dispersion of ruthenium on this solid presents very low values.

In the lanthanum oxide system, several chemical species can be present such as La_2O_3, $La(OH)_3$, $La_2(CO_3)_3$, and $La_2O_2(CO_3)$ [6–9]. The presence of certain phases (e.g. oxycarbonates) has been connected with the catalytic stabilities of lanthanum oxide supported Ni solids [10]. Moreover, a lanthanum oxide support can be formed from lanthanum carbonate phases [10,11] that could participate in the catalytic cycle of the dry reforming of methane. In the reaction mechanism proposed by Verykios et al. [10] for Ni/La_2O_3 and successfully applied for Rh and Ru/La_2O_3 catalysts [11,12], methane reversibly adsorbs on the metallic clusters while the cracking of the adsorbed species proceeds slowly liberating H_2 and generating carbon that remains on the metallic surface. The CO_2 rapidly reacts with La_2O_3 to generate oxycarbonate which in turn reacts slowly with carbon to generate carbon monoxide. This slow reaction could most likely occur at the metal/support interface.

* Corresponding author. Tel.: +54 342 4536861; fax: +54 342 4536861.
E-mail addresses: lmcornag@fiq.unl.edu.ar, lcornaglia2002@yahoo.com (L.M. Cornaglia).

0926-3373/$ – see front matter © 2013 Elsevier B.V. All rights reserved.
http://dx.doi.org/10.1016/j.apcatb.2013.12.005

In a previous study [13], we reported a Ru catalyst supported on lanthanum oxycarbonate with high surface area for use in membrane reactors. In this case, the carbon dioxide and methane conversions were similar, suggesting that this solid does not favor the reverse water gas shift reaction (RWGS) for DRM conditions in a membrane reactor at a reaction temperature as low as 550 °C [13].

The goal of the present work is to study the structure and reactivity of Ru and lanthanum species during reduction, re-oxidation and the combined reforming of methane (CRM; $CH_4 + CO_2 \leftrightarrow 2H_2 + 2CO$ and $CH_4 + ½\ O_2 \leftrightarrow 2H_2 + CO$). To accomplish this, we employed in situ laser Raman spectroscopy (LRS) complemented by pseudo in situ XPS. To our knowledge, in situ Raman spectroscopy has rarely been applied for investigating lanthanum compounds under reaction conditions, in particular, during methane reforming reactions.

All Ru catalysts were evaluated under two different reactor operations: differential regime to determine the reaction rates and under equilibrium conditions to measure carbon dioxide and methane conversions.

2. Experimental

2.1. Catalyst preparation

A high surface area lanthanum oxycarbonate phase was synthesized as support for Ru catalysts. La_2O_3 (Aldrich) was heated at 650 °C in pure O_2 flow (UAP 5.0) during 6 h to obtain pure La_2O_3 crystalline phase [14]. Then, a treatment with a solution of acetic acid (50% v/v) was performed, stirring and drying at 80 °C to evaporate the solution. After that, the solids were dried at the same temperature in a rotary evaporator (MR) during 6 h or in a vacuum oven (MV) during 12 h (Table 1). All supports were calcined at 400 °C in pure O_2 flow. The metal was added using a solution of $RuCl_3{\cdot}3H_2O$ by wet impregnation (Ru1) or by metal incorporation during the support synthesis (Ru2) (Table 1). The concentration of Ru was 0.6%w/w in all catalysts.

To prepare the $La_2O_2CO_3$-type II phase, La_2O_3 (Anedra) was heated under flowing dry CO_2 using a temperature program consisting of a linear 5 °C min^{-1} ramp from 25 to 650 °C, a linear 2 °C min^{-1} ramp from 650 to 700 °C, and finally an isothermal heating at 700 °C for 30 min [15]. The preparation of the $La_2O_2CO_3$-type Ia phase was performed by the thermal treatment of La_2O_3 (Aldrich 99.99% Gold Label). The oxide was heated at 10 °C min^{-1} from 25 to 500 °C under flowing He. The flow was then switched to dry CO_2 and the temperature kept at 500 °C for 1 h [15].

2.2. Catalyst characterization

2.2.1. Surface area

The BET (Brunauer, Emmett, and Teller) surface area was calculated from N_2 adsorption isotherms at liquid nitrogen temperature using a Quantachrome Autosorb automatic gas adsorption instrument. Prior to measurements, all samples were degassed at 150 °C under 0.13 Pa overnight.

Table 1
Summary of support and catalysts synthesized.

Solids	Drying	Ruthenium incorporation
MR	Rotary evaporator	–
MV	Vacuum oven	–
Ru2MR	Rotary evaporator	Support synthesis
Ru1MV	Vacuum oven	Wet impregnation
Ru2MV	Vacuum oven	Support synthesis

2.2.2. Metal dispersion

The metal dispersion of the fresh catalyst was determined by static equilibrium adsorption of CO at 25 °C in a conventional vacuum system, following the hydrogen reduction at 550 °C for 1 h. By taking the difference between the two isotherms, the amount of irreversibly adsorbed carbon monoxide was determined. The CO/Ru ratio was considered equal to one for the Ru dispersion estimation.

The following expression was employed to estimate the metallic dispersion (D_{Ru}):

$$D_{Ru}[\%] = \frac{N_{ads}^{T} - N_{ads}^{R}}{\text{mol Ru}}$$

N_{ads}^{T}: Total CO adsorbed [mol]
N_{ads}^{R}: Reversible CO adsorbed [mol].

2.2.3. X-ray diffraction (XRD)

The XRD patterns of the calcined solids and supports were obtained with an XD-D1 Shimadzu instrument, using Cu $K\alpha$ radiation at 30 kV and 40 mA. The scan rate was 1.0°/min for values between $2\theta = 10°$ and 70°.

2.2.4. Temperature-programmed reduction (TPR)

An Ohkura TP-20022S instrument equipped with a TCD was used for the TPR experiments. To carry out a thermal treatment similar to the one performed in the reaction system, the samples were heated up to 550 °C in nitrogen flow, kept constant for one hour, and then cooled down in N_2 flow. Afterwards, they were reduced in a 5% H_2–Ar stream with a heating rate of 10 °C min^{-1} up to the maximum treatment temperature.

In addition, the evolved gases were analyzed with an on-line Shimadzu GCMS-QP 2000/QP-2000 quadrupole mass spectrometer. The masses corresponding to water and carbon dioxide were followed.

2.2.5. Laser Raman spectroscopy (LRS)

The Raman spectra were recorded using a LabRam spectrometer (Horiba–Jobin–Yvon) coupled to an Olympus confocal microscope (a 100 × objective lens was used for simultaneous illumination and collection), equipped with a CCD detector cooled to about −73 °C using the Peltier effect. The excitation wavelength was in all cases 532 nm (Spectra Physics diode pump solid state laser). The laser power was set at 30 mW. Integration times ranged from a few seconds to a few minutes, depending on the sample.

In situ LRS measurements were performed on a Linkam high temperature cell. The catalyst was loaded in powder and the feed flowed through the solids. The feed mixtures were prepared in a flow system built for this purpose.

In the Raman cell, different treatments were carried out as follows:

(i) The catalysts were exposed to 5% H_2/Ar flux at different temperatures between 25 and 550 °C. After that, the temperature was kept at 550 °C during 2 h. Subsequently, the gas was switched to a 30% CO_2/Ar mixture at 550 °C for 15 and 25 min.
(ii) After reduction at 550 °C, the catalysts were exposed to a mixture of 20% CH_4, 18% CO_2, 15% CO, 10% H_2 and Ar at different reaction times.
(iii) After reduction at 550 °C, the catalysts were exposed to a DRM reactant mixture with a composition of 10% CH_4, 10% CO_2 and Ar at different reaction times.
(iv) After reduction at 550 °C, the catalysts were exposed to a CRM reactant mixture with a composition of 10% CH_4, 10% CO_2, 3.3% O_2 and Ar at different reaction times.

2.2.6. X-ray photoelectron spectroscopy (XPS)

The XPS measurements were carried out using a multi-technique system (SPECS) equipped with a dual Mg/Al X-ray source and a hemispherical PHOIBOS 150 analyzer operating in the fixed analyzer transmission (FAT) mode. The spectra were obtained with pass energy of 30 eV; an Mg-$K\alpha$ X-ray source was operated at 200 W and 12 kV. The working pressure in the analyzing chamber was less than 5.9×10^{-7} Pa. The XPS analyzes were performed on the supports and on the solids after treatment with H_2 or CO_2 at 400 °C carried out in the reaction chamber of the spectrometer. The spectral regions corresponding to La 3d, C 1s, O 1s, Ru 3d and Ru 3p core levels were recorded for each sample. All photoelectron binding energies were referenced to the C1s peak of adventitious carbon, set at 284.6 eV.

The data treatment was performed with the Casa XPS program (Casa Software Ltd, UK). The peak areas were determined by integration employing a Shirley-type background. Peaks were considered to be a mixture of Gaussian and Lorentzian functions in a 70/30 ratio. For the quantification of the elements, sensitivity factors provided by the manufacturer were used.

2.3. Catalytic test

2.3.1. Reaction rate measurements

The catalyst (50 mg) was loaded into a tubular quartz reactor (inner diameter, 5 mm) which was placed in an electric oven. The catalysts were heated in Ar at 550 °C and then reduced in situ in flowing H_2 at the same temperature for 2 h.

The stability tests were carried out at $W/F = 2.67 \times 10^{-5}$ g h ml^{-1} under differential conditions.

The total gas flow rate was varied using a weight of 10 mg of catalyst and 50 mg of quartz to select working conditions with no limitations of external mass transfer.

The forward rate of reaction (r_f) was calculated from the net rate of reaction (r_n) by:

$$r_f = r_n (1 - \eta)$$

$$r_n = \frac{F_{A0} X_A}{W}$$

$$\eta = \frac{(P_{CO})^2 \left(P_{H_2}\right)^2}{\left(P_{CH_4}\right)\left(P_{CO_2}\right)} \frac{1}{K_e}$$

where F_{A0} is the feed molar flux of A species, X_A is the conversion of A species, W is the catalyst mass, P_i are the prevalent pressures of reactants and products and K_e is the equilibrium constant calculated at the corresponding reaction temperature. The calculated η values were lower than 0.005 confirming the quality of the differential data obtained.

The turnover frequency (TOF) was determined from the methane forward reaction rate (r_{CH_4}) and the Ru dispersion (D_{Ru}) by the following expression:

$$\text{TOF}\left[\frac{1}{S}\right] = \frac{r_{CH_4}[\text{mol CH}_4/\text{mol Ru.S}]}{D_{Ru}}$$

2.3.2. Conversions under equilibrium conditions

The catalyst (200 mg) was loaded into a tubular quartz reactor (inner diameter, 16 mm) and placed in an electric oven. The catalysts were heated up to 550 °C in Ar flow and then reduced in H_2 flow at the same temperature for 2 h. The methane reforming reactions were performed at 550 °C employing the following feed flow [CH_4:CO_2:O_2:Ar] ratios equal to [1:1:0:1.2] and [1:1:0.3:0.9]. The O_2 concentration was 10% and $W/F = 2 \times 10^{-4}$ g h ml^{-1} in these experiments.

The feed gases and the reaction products for both flow conditions were analyzed with two on-line thermal conductivity detector gas chromatographs: a Shimadzu GC-8A and a SRI 8610C (SRI Instruments (USA)). The former instrument was equipped with a Porapak column, and the latter with a molecular sieve column. The carbon balance was close to one in all cases.

3. Results and discussion

3.1. Supports characterization

Fig. 1 shows the X-ray diffraction patterns of La_2O_3 and of the synthesized MR and MV supports, dried in a rotary evaporator or in a vacuum oven, respectively. The La_2O_3 diffractogram exhibits reflections assigned to hexagonal La_2O_3 (JCPDS 74-2430) and small signals from the $La(OH)_3$ phase (JCPDS 6-585).

Three polymorphic crystalline forms of $La_2O_2(CO_3)$ can be observed. All are layer-type structures built up of slabs of $(La_2O_2^{2+})_n$ polymers and CO_3^{2-} groups. Type-I has the square $(La_2O_2^{2+})_n$ layers found in LnOCl and related compounds (tetragonal), while type-II has the hexagonal $(La_2O_2^{2+})_n$ layers found in the A-form sesquioxides. Type-Ia, on the other hand, has monoclinic form [9]. In the case of the MR support, the diffractogram shows signals assigned to the monoclinic $La_2O_2CO_3$-type Ia phase and also low intensity reflections from $La(OH)_3$. However, in the XRD diffraction pattern of the MV support, only the monoclinic $La_2O_2CO_3$-type Ia phase could be observed.

Laser Raman spectroscopy has proved to be a useful technique to distinguish among different lanthanum phases. Raman spectra, taken for the reference phases and the synthesized supports in the 200–1150 cm^{-1} region, are shown in Fig. 2. In a previous study, the structure of pure lanthanum phases was studied by laser Raman spectroscopy, XRD and FTIR [15]. Those results are summarized in Table 2. The bands in the 350–400 cm^{-1} region were assigned to fundamental modes of La–O. In addition, the bands in the 700–1500 cm^{-1} region corresponded to the vibration of the CO_3^{2-}groups.

The spectrum of lanthanum hydroxide shows four bands at 274, 339, 447, and 597 cm^{-1}. The frequencies of these bands agree with those reported for the crystalline phase of $La(OH)_3$ [16]. The Raman spectrum of $La_2O_2CO_3$-type II shows two peaks in the region of 200–600 cm^{-1}, at 358 and 384 cm^{-1} (Fig. 2). It presents a strong signal at 1086 cm^{-1} and other weak bands at 1408, 1415, and 1450 cm^{-1}. The spectrum of $La_2O_2CO_3$-type Ia has several

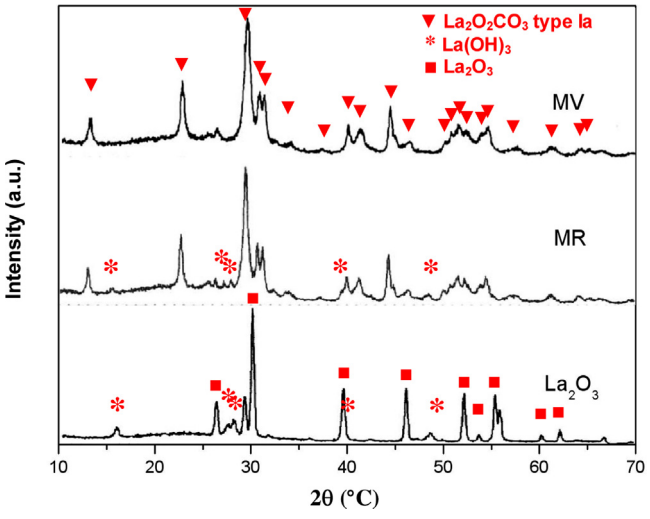

Fig. 1. XRD pattern of La_2O_3 and MR and MV supports.

Table 2
XRD phases and Raman shift of lanthanum compounds [15] and supports.

XRD phase (N° ASTM)	Vibration frequencies—laser Raman spectroscopy				
	250–700 cm^{-1} region	700–1500 cm^{-1} region (CO_3^{2-})			
Ia–$La_2O_2CO_3$(48-1113)	294, 315, 340, 356, 387, 437 (sh), 450	1340, 1417, 1444	1057, 1089	852	707, 737
$La(OH)_3$(6-585, 36-1481)	284, 339, 447, 597	–	–	–	–
La_2O_3 (5-602)	400	–	–	–	–
II-$La_2O_2CO_3$(37-804)	358, 384	1408, 1415, 1450	1087	–	747
MV	298, 317, 336, 358, 440, 455		1053, 1062		
MR	298, 317, 336, 358, 440, 455		1053, 1062		

overlapping peaks at 294, 315, 338, 356, 387, and 437 (sh), 450 cm^{-1}. In addition, multiple splitting is observed in the 700–1150 cm^{-1} region (Fig. 2). The strongest band appears at 1060 cm^{-1}.

MR and MV supports calcined at 400 °C present $La_2O_2CO_3$-type Ia as the main phase. Furthermore, the spectra show weak bands at 284, 342, and 452 cm^{-1} that reveal the presence of small amounts of $La(OH)_3$ (Table 2).

3.2. Characterization of calcined Ru catalysts

Fig. 3 shows the X-ray diffraction patterns of the Ru catalysts, where the peaks assigned to the $La_2O_2CO_3$-type Ia phase are observed. Therefore, it can be noticed that the incorporation of the noble metal did not produce a phase change in the supports. Besides, reflections from Ru oxides were not detected in the calcined catalysts by XRD. This result suggests that the average crystallite size of the Ru species was below the XRD detection limit and the oxidized Ru species were well dispersed on the support structure.

Fig. 4 shows the Raman spectra of fresh catalysts compared with the calcined supports. It can be seen that after the incorporation of metal, all solids kept the same structure in agreement with the X-ray diffraction data. In addition, all catalyst spectra

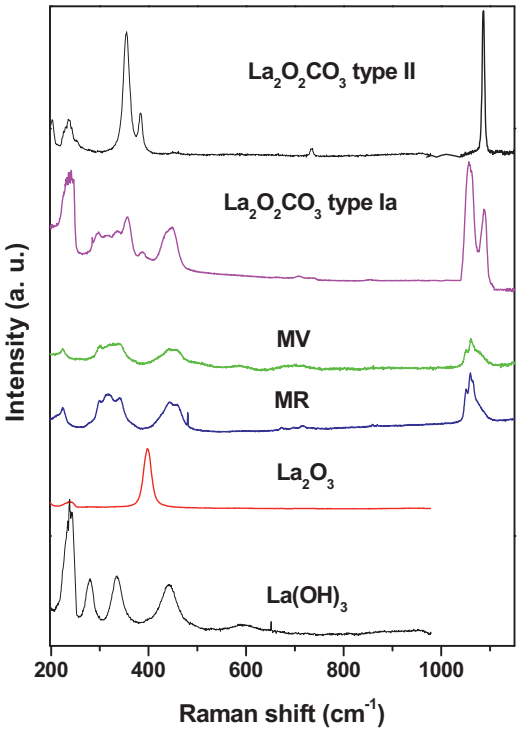

Fig. 2. Raman spectra of La_2O_3, MR, MV supports and reference phases ($La_2O_2CO_3$ type Ia and II).

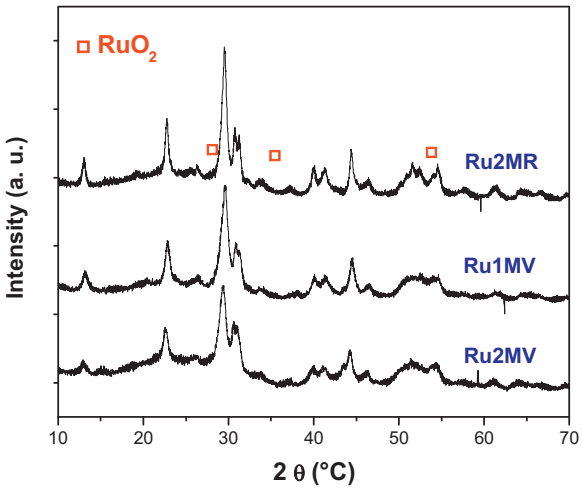

Fig. 3. X-ray diffraction patterns of calcined Ru catalysts.

show a broad signal in the 600–700 cm^{-1} region which could be related to the presence of RuO_x oxides. For the freshly electrodeposited Ru film [17], a pair of bands at 470 and 671 cm^{-1} was observed in the Raman spectrum. These bands were assigned to different stretching modes of hydrated RuO_2. The RuO_3 formation included the appearance of a band at 800 cm^{-1} and the presence of RuO_4 was assumed from the formation of a band at 875 cm^{-1}. In our calcined catalysts, two overlapping signals at 622 and 670 cm^{-1} were observed which could be assigned to different stretching modes of RuO_x species (Fig. 4) and no peaks were detected close to 800 cm^{-1}. The broad Raman band at 670 cm^{-1} was previously attributed to Ru(III) which strongly interacts with La [5].

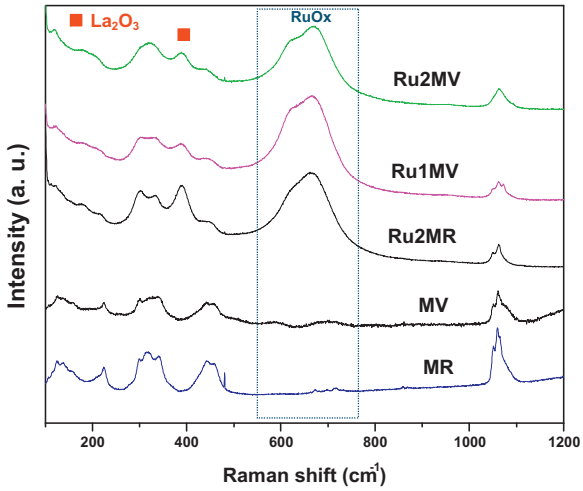

Fig. 4. The Raman spectra of the MR and MV supports and ruthenium catalysts.

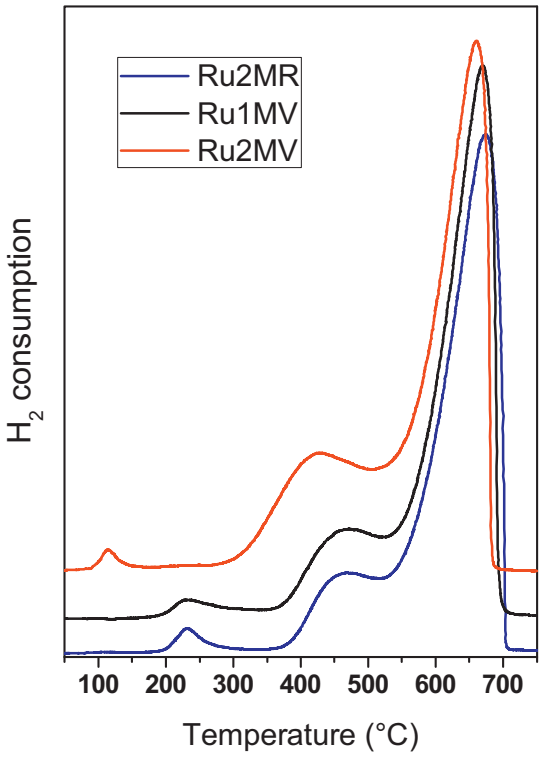

Fig. 5. TPR profiles of Ru catalysts pre-treated in N_2 flux at 550 °C.

To study the reducibility of Ru species, temperature-programmed reduction experiments were carried out. The calcined solids were pre-treated in situ in N_2 flow at 550 °C (Fig. 5). All profiles exhibited two minor peaks of reduction at about 200 and 500 °C and a third major peak at a higher temperature (600–700 °C). In order to separate the contributions of the 350–700 °C region, a TPR experiment coupled to a mass spectrometer was performed. Signals at amu = 44 and 18 were observed in the mass spectrometer profile. These results indicate that the peak at low temperature ($T < 260$ °C) could be assigned to a reduction of Ru oxide particles. However, the hydrogen consumption peak between 400 and 500 °C was due to a ruthenium oxide particles reduction, and also to the decomposition of $La(OH)_3$ and carbonate species. Furthermore, the peak in the 600–700 °C region could be assigned to the $La_2O_2CO_3$ decomposition. It is known that the decomposition temperatures of lanthanum hydroxide and carbonate compounds are between 400 and 800 °C, respectively [18].

In previous studies of Ru/La_2O_3 solids, we compared TPR profiles of solids with different contents of ruthenium [5]. For the catalysts with lower metal contents (Ru(0.2) and Ru(0.6)) both profiles were similar. The samples show a main reduction peak at 260 °C, a second one a 375 °C, and a low-intensity shoulder at 140 °C.

Yan et al. [19] reported two reduction peaks at 150 and 200 °C in Ru/SiO_2 catalysts. The low temperature peak was assigned to well-dispersed RuO_x species and the high temperature peak was attributed to RuO_2 particles [19]. The high temperature peak at 260 °C in Ru(0.2) and Ru(0.6) solids supported on La_2O_3 suggested the presence of a strong metal–support interaction. And the very low-intensity of the 140 °C peak was in agreement with the low dispersion of all solids [5].

In addition, in our previous studies of Ru/La_2O_3 solids, laser Raman spectroscopy and TPR results indicated the presence of Ru(III) strongly interacting with Type II lanthanum oxycarbonate [5].

Table 3
Surface area, Ru dispersion and reaction rates for CH_4–CO_2 reaction at 550 °C of Ru catalysts.

Solids	r_{CH_4} [a]	r_{CO_2} [a]	H_2/CO	D[%] [b]	TOF [s^{-1}]	Sg fresh [$m^2\,g^{-1}$]	Sg used [c] [$m^2\,g^{-1}$]
Ru/La_2O_3 [d]	0.21	0.44	0.29	7	14	5–7	–
Ru2MR	0.25	0.59	0.30	18	6.5	35.2	22.1
Ru1MV	0.23	0.43	0.30	19	5.6	31.4	16.3
Ru2MV	0.25	0.48	0.28	14	8.1	33.4	17.6

[a] r_{CH_4} and r_{CO_2} [$mol\,h^{-1}\,g\,cat^{-1}$] were measured after 24 h on stream. $W/F = 2.67 \times 10^{-5}$ g h ml^{-1}
[b] Dispersion determined from CO chemisorptions.
[c] Surface area measured in used catalysts after 90 h in reaction conditions.
[d] From Ref. [2].

3.3. Reaction rates and stability for the dry reforming of methane (DRM)

The activity and stability of the Ru catalyts were evaluated in a conventional fixed-bed reactor for the DRM reaction under differential conditions. Table 3 shows the reaction rate and H_2/CO ratio of Ru supported on lanthanum oxycarbonate compared with the Ru/La_2O_3 catalyst. The surface area values of catalysts before (fresh) and after (used) the catalytic test are also summarized in Table 3.

The La_2O_3 surface area was 5 $m^2\,g^{-1}$. From the pure lanthanum oxide crystalline phase treated with acetic acid, lanthanum oxycarbonates with high surface area were obtained. When the solid was dried in a rotary evaporator (MR), a surface area of 15.1 $m^2\,g^{-1}$ was reached after calcination at 400 °C whereas after drying the samples in a vacuum oven (MV), the value obtained was 26.5 $m^2\,g^{-1}$. These surface areas increased further after the incorporation of ruthenium, reaching values between 30 and 35 $m^2\,g^{-1}$ (Table 3) and after being under reaction conditions for 90 h, they decreased up to 16–22 $m^2\,g^{-1}$.

The metal dispersion of the catalysts was measured by CO chemisorption at room temperature. For the three catalysts, dispersions between 14 and 19% were obtained. As Ru dispersion and the reaction rate had similar values for the $Ru/La_2O_2CO_3$ catalysts, the calculated turnover frequencies (TOF_{CH_4}) were also similar, within the 5.6–8.1 s^{-1} range. In a previous paper, we also reported a TOF value close to 4 s^{-1} at 550 °C with a Ru dispersion of 0.24 [2] for Ru/La_2O_3–SiO_2 catalysts.

The turnover frequencies for the dry methane reforming experiments were in reasonable agreement with the TOFs, reported in the literature for Ru catalysts [2,20,21]. Jakobsen et al. [21] studied steam and CO_2 reforming of methane over Ru/ZrO_2, their data were well described by a kinetic model assuming the partial blockage of the active sites by adsorbed CO and H. Rostrup-Nielsen and Hansen [22] proposed a factor of 2–3 lower activities for CO_2 reforming in comparison with steam reforming. Then, the TOF of 11 s^{-1} for steam reforming at 500 °C over a Ru/ZrO_2 catalyst reported by Jakobsen et al. [21] would expect values of 4 and 6 s^{-1} during CO_2 reforming. These estimated values are close to the TOF reported in the present paper. However, Wei and Iglesia [23] found that turnover frequencies values on CH_4 reforming were independent of the co-reactant (CO_2 or H_2O) employed. These similarities in turnover rates for the two CH_4 reforming would indicate a common kinetically relevant step, which cannot involve species derived from co-reactants. They studied CH_4 reforming over Ru, Rh, Pt and Ir catalysts [23]. For Ru catalysts, with similar dispersion, they found lower values than those previously reported for dry refoming of methane at 600 °C.

Furthermore, the H_2/CO ratio was similar for all Ru catalysts. This ratio was also calculated from the methane and carbon dioxide

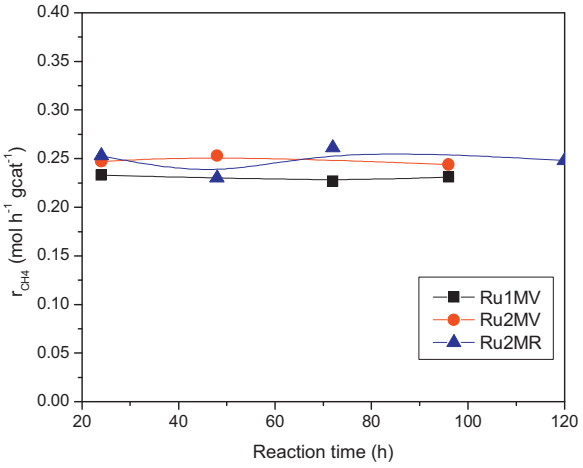

Fig. 6. Stability test of Ru catalysts after reduction at 550 °C in the fixed-bed reactor. (Reaction temperature = 550 °C, W/F = 4.3×10^{-6} g h ml^{-1}) Feed composition: P_{CH_4} : P_{CO_2} : P_{Ar} = 1 : 1 : 1.1.

reaction rates and these values were close to the measured values in all cases. The low values (H_2/CO = 0.30) give evidence of the occurrence of the reverse water gas shift reaction, simultaneously with the dry reforming of CH_4. It should be equal to one if only the dry reforming reaction occurred.

Fig. 6 shows the stability of the catalysts for the DRM reaction. All catalysts were stable after 90 h in reaction. In addition, the solids exhibited higher reaction rate values than Ru/La_2O_3. No differences in the catalytic activity were observed between the catalysts synthesized employing different drying steps (Ru2MV and Ru2MR). Comparing Ru1MV and Ru2MV catalyts, it can be observed that Ru1MV (prepared by wet impregnation) showed a slightly lower TOF.

3.4. Carbon dioxide and methane conversions for the dry and combined reforming of methane under equilibrium conditions

The Ru/$La_2O_2CO_3$ catalytic activity for the dry reaction of methane followed by oxygen addition (CRM) was measured. These measurements were carried out with a 0.8 cm catalyst bed and high W/F. Under such conditions, the system could reach thermodynamic equilibrium.

In the case of the addition of oxygen to the feed mixture, an increase in CH_4 conversion and H_2 production could be achieved. The reactions that might occur were the following: the partial oxidation of methane (POM) and the dry reforming reaction (DRM) in addition to total oxidation of methane ($CH_4 + 2O_2 \leftrightarrow 2H_2O + CO_2$) and the reverse (RWGS) or direct water gas shift reaction. Table 4 shows the measured methane and carbon dioxide conversions in comparison with simulated values by HYSYS software for both feed compositions, DRM and CRM.

To calculate the data, we employed the same total flow used in laboratory experiments. Even the dimensions given to the Gibbs reactor, applied for the thermodynamic equilibrium calculations, were equal to those used in the laboratory.

The methane conversion increased while the carbon dioxide conversion decreased when oxygen was added to the mixture, as expected, due to the occurrence of the total oxidation of methane. In the reactor outlet, oxygen was not chromatographically detected, indicating that it was completely consumed in the 0.8 cm catalytic bed.

As shown in Table 4, values close to equilibrium were achieved in all conditions in the Ru2MR and Ru1MV catalysts. In the case of CRM, a different behavior was observed between the Ru2MV and Ru2MR catalysts. The Ru2MVsolid showed a methane conversion lower than the equilibrium value; however, values close to equilibrium were reached under DRM conditions. Note that Ru was incorporated during the support synthesis in both solids.

3.5. Reduction–reoxidation of Ru species supported on $La_2O_2CO_3$ followed by in situ LRS and pseudo in situ XPS

To investigate how RuO_x species and lanthanum phases changes under reducing and oxidizing conditions, their transformations were followed by in situ laser Raman spectroscopy during several treatments. Fig. 7 shows the Raman spectra of the catalysts exposed to 5% H_2/Ar flux at different temperatures between 25 and 550 °C. After that, the temperature was kept at 550 °C during 2 h and then the solid was exposed to 30% CO_2/Ar mixture for 25 min.

At room temperature, the spectra show a signal in the 600–700 cm^{-1} region, assigned to Ru (III) oxide and the bands corresponding to the oxycarbonate-type Ia phase (296, 335, 448 and 1060 cm^{-1}) (Fig. 7). For all solids, the broad signal at 670 cm^{-1} disappeared when the temperature increased up to 400 °C, showing the reduction of Ru species in agreement with TPR data.

In addition, a signal at 400 cm^{-1} assigned to La_2O_3 was observed at room temperature for the Ru1MV solid. During the reduction treatment, the oxycarbonate bands were gradually removed and only one peak was observed at 400 °C. This result shows that almost all the oxycarbonate was decomposed at this temperature. For the other solids, the signals assigned to lanthanum oxycarbonates were always observed during the reduction process up to 400 °C. However, after two hours at 550 °C, the signals disappeared indicating the complete decomposition of the oxycarbonates. Note that in the Ru1MV catalyst, the lanthanum oxycarbonate decomposes at lower temperatures.

Subsequently, the gas was switched to a 30% CO_2/Ar mixture at 550 °C (Fig. 7). The carbon dioxide composition was similar to that employed in the dry reforming of methane reaction. In this experiment, it was found that the ruthenium particles were re-oxidized because there appeared the broad signal assigned to RuO_x. The La_2O_3 signal did not change during the time during which the experiment took place (25 min).

A similar effect was observed in the Ru/La_2O_3 catalysts on CO_2 rich streams by in situ Raman measurements [12]. The partial re-oxidation of metallic Ru was assigned as one of the factors that produced the catalyst deactivation under such conditions. Matsui et al. [24] studied the effect of the support on the activity and reaction mechanism in the CO_2 reforming of methane over Ru/La_2O_3

Table 4
Catalytic behavior of Ru/$La_2O_2CO_3$ in a conventional fixed-bed reactor for different feed gas compositions.

Ratios CO_2:CH_4:O_2:Ar	Ru1MV		Ru2MV		Ru2MR		Equilibrium values[b]	
	X_{CH_4}[a]	X_{CO_2}[a]	X_{CH_4}	X_{CO_2}	X_{CH_4}	X_{CO_2}	$X_{CH_{4eq}}$	$X_{CO_{2eq}}$
1:1:0:1.2	27.6	40.1	27.8	37.0	28.8	36.0	30.7	41.6
1:1:0.3:0.9	42.3	10.1	34.1	14.2	42.1	11.1	47.2	12.5

[a] Methane and carbon dioxide conversions, catalyst mass = 0.2 g, W/F = 2×10^{-4} g h ml^{-1}, reaction temperature = 550 °C.
[b] Calculated using HYSYS 3.0 software.

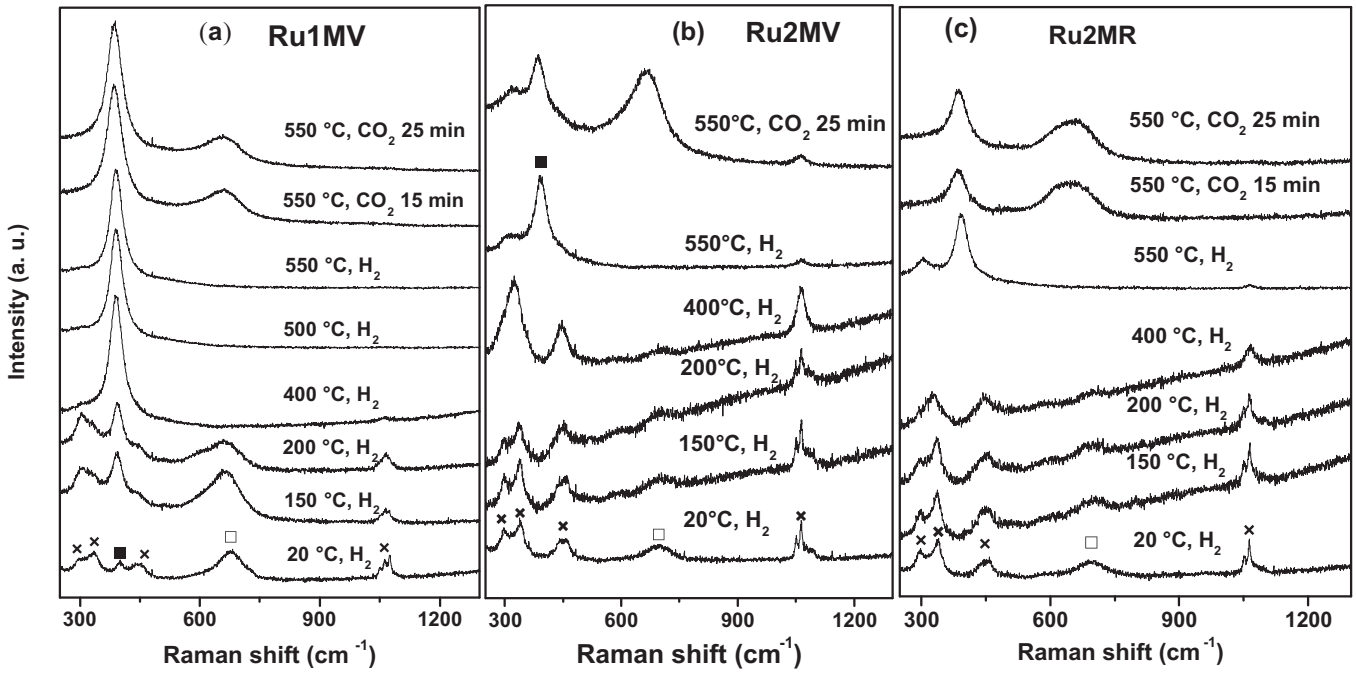

Fig. 7. In situ LRS of Ru catalytic systems exposed to a reducing atmosphere (5% H_2/Ar) and oxidant (30% CO_2/Ar) at different times and temperatures. References: RuO_x (□), La_2O_3 (■) and $La_2O_2CO_3$-type Ia (×).

catalysts. They proposed the following reaction step based on CO_2 pulse experiments:

$$Ru/La_2O_3 + CO_2\,(ad) \Rightarrow CO\,(gas) + Ru - O_X/La_2O_3$$

In the same way, other authors reported the oxidation of Ru particles under oxygen at 600 °C in Ru/SiO_2 [19] and Ru/Al_2O_3 [25] catalysts.

The reduction/oxidation effect on surface Ru species was also studied by XPS measurements. In this experiment, the solids were exposed to H_2 and CO_2 flux in the reaction chamber of the spectrometer at 400 °C. In a first stage, the catalysts were exposed to 5% H_2/Ar flow at 400 °C and then they were kept at this temperature for 10 min. The Ru 3p, Ru 3d, C 1s, O1s and La 3d regions were recorded.

Fig. 8a shows the Ru 3d XPS spectra obtained on the reduced catalysts. There is an overlap between the signals of the Ru 3d and C1s peaks at 284.6 eV, the latter being due to carbonaceous contamination. The peak at 289.2 eV was assigned to carbonate (CO_3^{2}), while Ru^0 species appeared at 280.1 eV. Because of this overlap, the Ru $3p_{3/2}$ signal was also analyzed. The binding energy at 462 eV confirms the complete surface reduction to Ru^0 in all catalysts after treatment in H_2 at 400 °C.

The O 1s region showed two signals at 531.5 and 528.9 eV (not shown). The first peak could be related to C–O and/or O–H species and the second to O^{2-} of the framework [26]. For all catalysts, the intensity of the high binding energy peak was twice as much that of the low binding energy signal. In addition, the La $3d_{5/2}$ core level was observed at 833.6 eV and the corresponding satellite-split was 3.9 eV with a well-resolved profile. These values agree well with those previously reported by Chan and Bell [16] for La_2O_3.

Table 5 summarizes the XPS intensity ratios of reduced Ru catalysts. The ruthenium surface ratio (Ru3p/La) was higher when the metal was incorporated by wet impregnation. Note that in this solid, the lanthanum oxycarbonate decomposes at lower temperature (Fig. 7). The CO_3^{2-}/La and O1s/La surface ratios were similar for all catalysts. In addition, for the three catalysts, the CO_3^{2-}/O^{531} ratio was close to 0.33 indicating that carbonate species are always present on the surface.

Subsequently, the catalysts were exposed to 30% CO_2/Ar flow at 400 °C during 10 min. Fig. 8b shows the Ru 3d XPS spectra obtained on the catalysts. The Ru $3d_{3/2}$ signal was shifted to higher binding energy for Ru1MV and Ru2MV, suggesting that Ru particles were re-oxidized in these solids. This binding energy shift was not observed in the Ru2MR solid, indicating that the Ru oxidation state did not change at this temperature. Note that this experiment was performed at lower temperature than LRS experiments due to the maximum temperature limit of the spectrometer reaction chamber.

3.6. *In situ laser Raman spectroscopy during the dry reforming of methane with and without oxygen addition*

To further understand how the reaction mixture interacts with Ru and lanthanum species, the catalysts were exposed to a mixture of 20% CH_4, 18% CO_2, 15% CO, 10% H_2 and Ar in a high temperature cell and their changes were monitored by in situ LRS. The mixture composition was similar to that obtained in a fixed-bed reactor with high W/F, which allowed reaching thermodynamic equilibrium for the dry reforming of methane.

Fig. 9 shows the Raman spectra of the Ru1MV and Ru2MV catalysts reduced in situ at 550 °C and exposed to this mixture. After reduction at 550 °C, only the band at 400 cm^{-1} corresponding to lanthanum oxide was observed for both catalysts. When the reducing atmosphere was changed to the reaction mixture, there

Table 5
Pseudo in situ XPS of Ru solids treated in H_2/Ar and CO_2/Ar mixtures at 400 °C.

Solid	Treatment	Ru3p/La	O^{531}/La	$C_{(CO_3)_2-}/O^{531}$	$C_{(CO_3)_2-}$/La
Ru2MR	H_2	0.005	1.17	0.44	0.52
	CO_2	0.006	1.30	0.43	0.55
Ru1MV	H_2	0.048	1.40	0.40	0.53
	CO_2	0.046	1.51	0.40	0.60
Ru2MV	H_2	0.008	1.20	0.37	0.45
	CO_2	0.011	1.48	0.45	0.67

For all samples, the binding energies of C and La were the following: C 1s = 284.8 eV, La $3d_{5/2}$ = 834.9 eV.

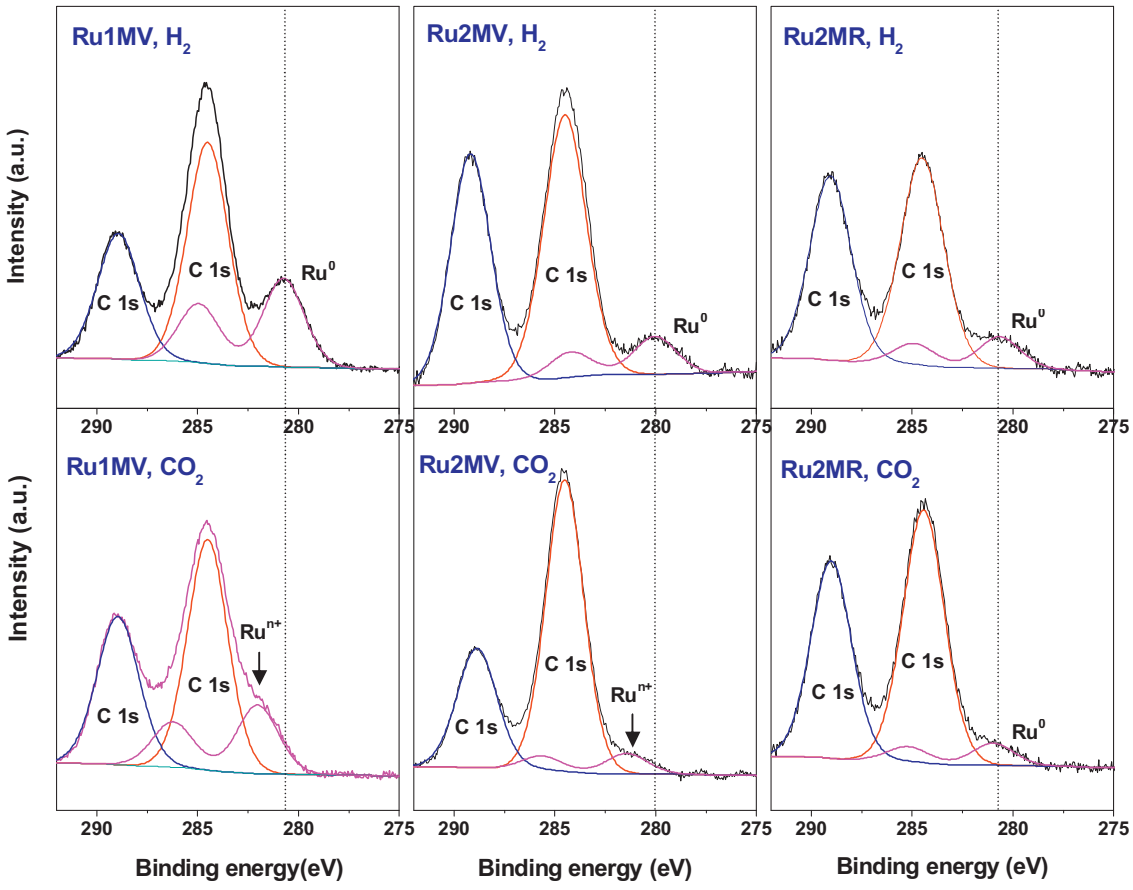

Fig. 8. XPS spectra of the catalysts exposed to a reducing atmosphere (H_2 (5%)–Ar) and oxidant (CO_2 (30%)–Ar) at 400 °C in the reaction chamber of the instrument.

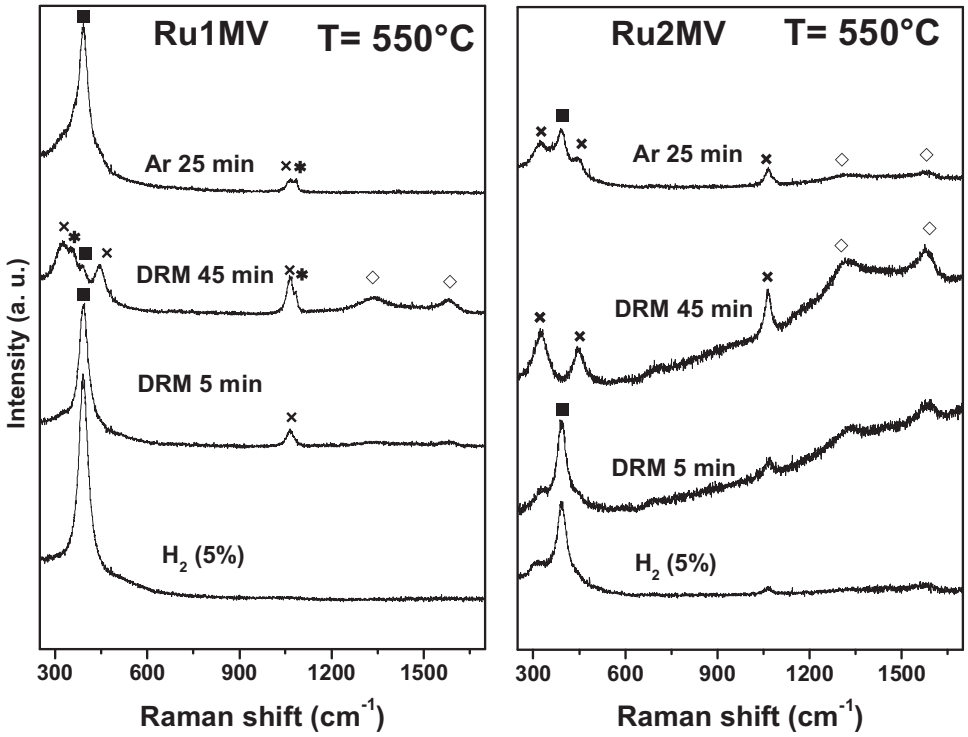

Fig. 9. In situ LRS of Ru catalytic systems exposed to a reactant mixture with a composition of 20% CH_4, 18% CO_2, 15% CO, 10% H_2 and Ar at 550 °C. References: La_2O_3 (■), $La_2O_2CO_3$-type Ia (×) and $La_2O_2CO_3$-type II (*).

appeared the signals corresponding to graphitic carbon at 1590, 1620 and 1350 cm^{-1}, their intensities increasing with the reaction time. The band at 1590 designated as *G* peak was the E2g mode of bulk graphite and its intensity scaled with the crystal size. The feature near 1340 cm^{-1}, designated as *D* (disorder) band, occurred near the crystal edges and the low intensity band at 1620 (*D′* band) usually appeared as a shoulder and could be assigned to the graphite layers located at the boundary of the crystals [27–31].

After 45 min on reaction, the complete transformation of La_2O_3 to oxycarbonate-type Ia (bands at 296–450 and 1060 cm^{-1}) was observed for the Ru2MV solid. However, in the case of Ru1MV, the band at 400 cm^{-1} was still present. In addition, low intensity bands assigned to lanthanum oxycarbonate-type II phase were detected for this solid.

To analyze the role of oxycarbonates on the reaction mechanism, the reaction mixture was changed to an inert gas (Fig. 9). Both the disappearance of the graphitic carbon bands at 1339 and 1590 cm^{-1} simultaneously and the appearance of the signal at 400 cm^{-1} assigned to La_2O_3 could be observed. Lanthanum oxide could be formed by the reaction of oxycarbonate with carbon deposited on the active sites of the catalyst releasing carbon monoxide [12]. This was one of the steps proposed in the reaction mechanism for Ni, Rh and Ru catalysts supported on La_2O_3 [10–12]. A complete picture of the proposed mechanism is shown below:

$$CH_4 + S \overset{K_1}{\longleftrightarrow} S - CH_4 \quad (1)$$

$$S - CH_4 \overset{k_2}{\longrightarrow} S - C + 2H_2 \quad (2)$$

$$CO_2 + La_2O_3 \overset{K_3}{\longleftrightarrow} La_2O_2CO_3 \quad (3)$$

$$La_2O_2CO_3 + C - S \overset{k_4}{\longrightarrow} La_2O_3 + 2CO + S \quad (4)$$

where S is the metallic site.

The in situ LRS study helps to support the key role assigned to the lanthanum oxycarbonate phase in the stability of lanthanum-based catalyts. This phase reacts with the carbon deposited on the catalyst surface avoiding the solid deactivation.

In a second experiment, all reduced catalysts were exposed to a DRM reactant mixture with a composition of 10% CH_4, 10% CO_2 and Ar and were monitored by in situ LRS at different reaction times. The Ru1MV solid showed a higher reactivity of lanthanum oxycarbonate to the formation of La_2O_3 in a hydrogen flow even at low temperatures (Fig. 7). This behavior could be related to the higher Ru/La surface ratio. When this solid was exposed to the reactant mixture, it was less reactive to the formation of lanthanum oxycarbonates suggesting that La_2O_3 was more stable (Fig. 10). Similar observations were reported for Pt and Rh catalyts after CO_2 treatments followed by ex-situ Raman and FTIR, where Pt would favour the carbon dioxide interaction with the support to form monoclinic polymorph (type Ia), while rhodium would prevent the further formation of the oxycarbonate phase [15].

In addition, the incipient formation of $La_2O_2CO_3$-type II phase was observed for the Ru1MV solid as evidenced by the appearance of the bands at 358 and 1089 cm^{-1}. After 50 min under reaction conditions, all catalysts showed the formation of graphitic carbon with characteristic signals at 1340 and 1590 cm^{-1}.

When oxygen was added to the reactant mixture (CRM conditions), the changes observed on the catalysts (Fig. 11) were more pronounced than for the dry reforming of methane. Note that the gas composition during the reaction should be different due to the total oxidation of methane that increased the CO_2 concentration decreasing the carbon dioxide conversion. In the case of the Ru1MV catalyst, the oxycarbonate-type II phase formation was observed.

Ru particles were partially re-oxidized for the Ru2MV solid under CRM conditions. The results obtained by Liu et al. [25] of in situ Raman after ignition of the partial oxidation of methane reaction showed that RuO_2 species were present even in the catalyst located at the top of the catalyst bed, where O_2 was still available in the reaction feed. This means that the noble metal species in the entire catalyst bed could be in a highly reduced form under the POM reaction conditions.

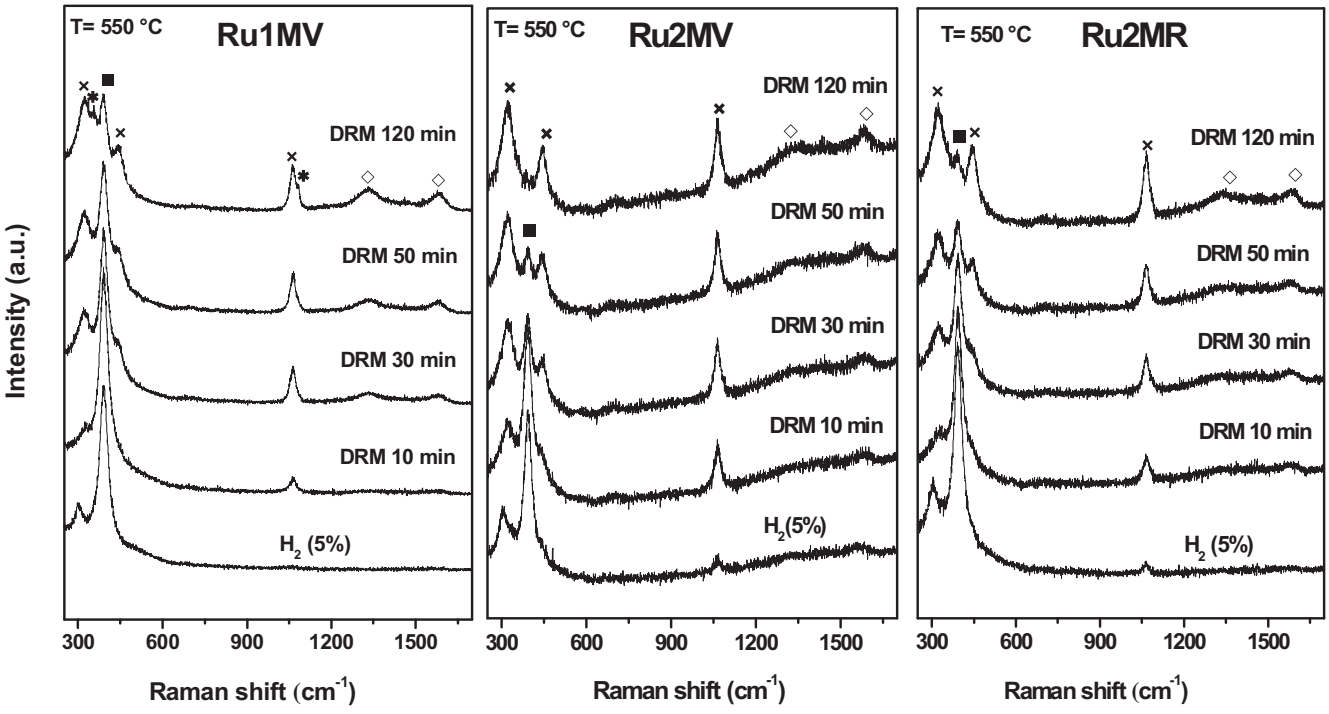

Fig. 10. In situ LRS of Ru catalytic systems exposed to a reactant mixture with a composition of 10% CH_4, 10% CO_2 and Ar at 550 °C. References: La_2O_3 (■), $La_2O_2CO_3$-type Ia (×) and $La_2O_2CO_3$-type II (*).

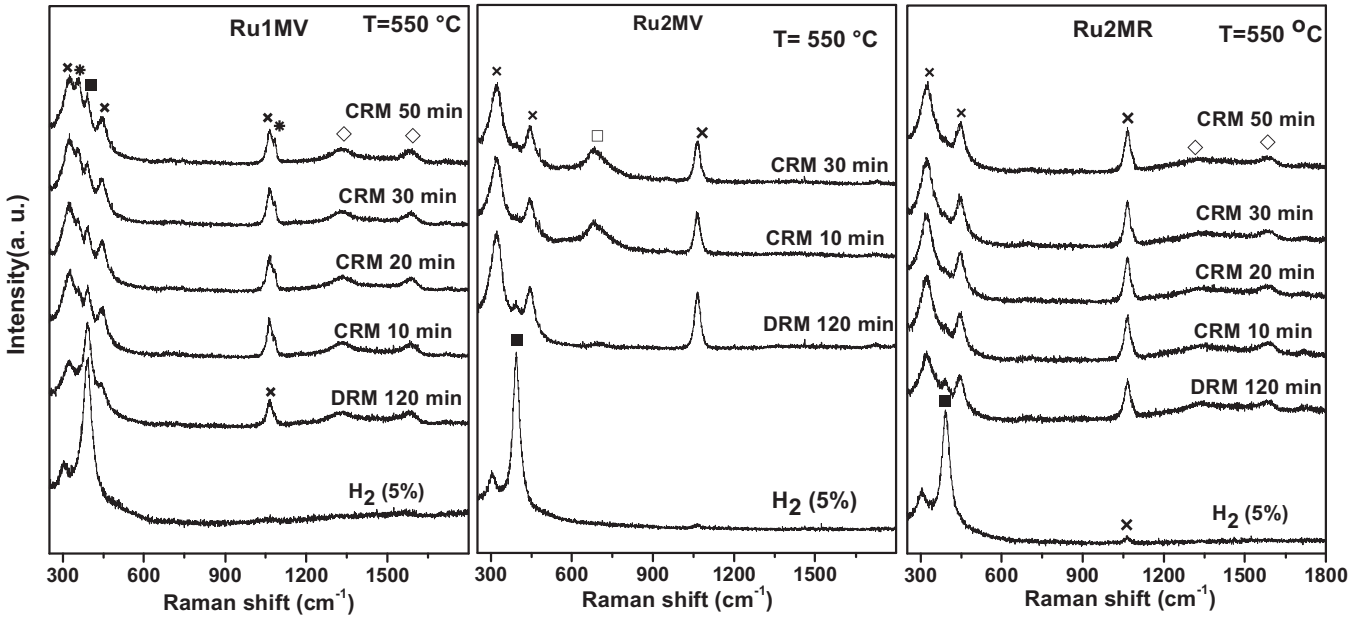

Fig. 11. In situ LRS of Ru catalytic systems exposed to a reactant mixture with a composition of DRM (10% CH_4, 10% CO_2 and Ar) and CRM (CH_4/O_2 = 3) at 550 °C. References: RuO_x (□), La_2O_3 (■), $La_2O_2CO_3$-type Ia (×) and $La_2O_2CO_3$-type II (*).

The change in Ru oxidation state is in agreement with the lowest activity of this catalyst in the combined reforming of methane under equilibrium conditions (Table 4).

To understand the catalytic behavior of the Ru1MV and Ru2MR solids in which no re-oxidation was observed during the combined reforming of methane (CRM), different thermal treatments were monitored by in situ LRS (Fig. 12). All experiments were carried out with the same methane and carbon dioxide mixture adding oxygen with a methane/oxygen ratio equal to three. After the reaction in CRM conditions, the Ru1MV and Ru2MR catalysts were exposed to an inert Ar flow during 10 min and the re-oxidation of the metallic ruthenium was observed. This could be due to decomposition of the lanthanum oxycarbonate producing CO_2, which re-oxidizes the Ru^0. After that, the solids were exposed again to the CRM mixture, the signals of the La_2O_3 and RuO_x species still being present in Ru1MV. Subsequently, this solid was exposed to the DRM mixture and the signal in the 600–700 cm^{-1} region disappeared, indicating the re-reduction to Ru^0. Furthermore, the incipient appearance of the oxycarbonate phase was observed.

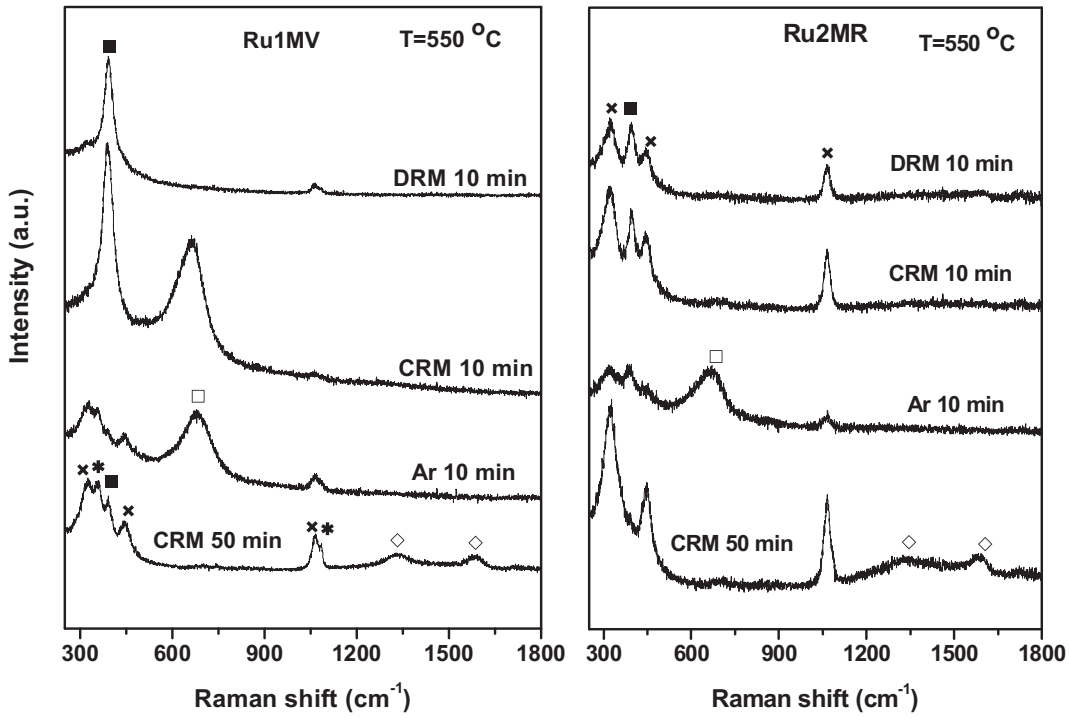

Fig. 12. In situ LRS of Ru catalytic systems exposed to different thermal treatments with cycles of Ar and the DRM and CRM reactant mixture at 550 °C. References: RuO_x (□), La_2O_3 (■), $La_2O_2CO_3$-type Ia (×) and $La_2O_2CO_3$-type II (*).

Table 6
Lanthanum and ruthenium species present in the catalysts exposed at different atmospheres, monitored by Raman spectroscopy.

Treatment	Catalyst			Figure
	Ru1MV	Ru2MV	Ru2MR	
H_2, 400 °C	Ru^0, La_2O_3	Ru^0, La_2O_3, $La_2O_2CO_3$-Ia	Ru^0, La_2O_3, $La_2O_2CO_3$-Ia	7
H_2, 550 °C	Ru^0, La_2O_3	Ru^0, La_2O_3	Ru^0, La_2O_3	7
CO_2, 550 °C	RuO_x, La_2O_3	RuO_x, La_2O_3	RuO_x, La_2O_3	7
DRM, 550 °C, 45 min (20%CH_4, 18% CO_2, 15% CO, 10%H_2 and Ar)	Ru^0, La_2O_3, $La_2O_2CO_3$-Ia and II, graphitic carbon (C)	Ru^0, La_2O_3, $La_2O_2CO_3$-Ia, C	–	9
Then, Ar,550 °C, 25 min	Ru^0, La_2O_3 (vs)[a], $La_2O_2CO_3$-Ia and II	Ru^0, La_2O_3, $La_2O_2CO_3$-Ia, C(t)[a]	–	9
DRM, 550 °C, 120 min (10%CH_4, 10% CO_2 and Ar)	Ru^0, La_2O_3, $La_2O_2CO_3$-Ia and II, graphitic carbon	Ru^0, La_2O_3, $La_2O_2CO_3$-Ia, C	Ru^0, La_2O_3, $La_2O_2CO_3$-Ia, C	10
DRM, 550 °C, 120 min CRM, 30 min	Ru^0, La_2O_3, $La_2O_2CO_3$-Ia and II, graphitic carbon	RuO_x, $La_2O_2CO_3$-Ia, C	Ru^0, $La_2O_2CO_3$-Ia, C(t)[a]	11
CRM, 50 min; Ar; CRM, 10 min, 550 °C	RuO_x, La_2O_3	–	Ru^0, La_2O_3, $La_2O_2CO_3$-Ia	12
Then, DRM, 550 °C, 10 min	Ru^0, La_2O_3 (vs)[a], $La_2O_2CO_3$-Ia (t)[a]	–	Ru^0, La_2O_3, $La_2O_2CO_3$-Ia	12

[a] (t) traces were detected; (vs) very strong.

In the case of the Ru2MR solid, when exposed to CRM conditions, the band at 670 cm^{-1} disappeared indicating that even under this condition the reduction to Ru^0 was observed.

3.7. *In situ structure–reactivity over Ru/lanthanum oxycarbonate*

The structural change and phase reactivity of Ru species supported on lanthanum oxycarbonates during methane reforming reactions were well followed by Raman spectroscopy.

The behavior of the catalysts was consistent with the reaction mechanism steps proposed for the Ru solid [12]. The species observed for each catalyst during the in situ LRS measurements are summarized in Table 6 where the most striking evidence obtained is highlighted. In the first experiment, the reduction of RuO_x species as a function of temperature was studied. Furthermore, the transformations of the lanthanum species were observed, which may be represented by the following reactions:

$$RuO_x + xH_2 \rightarrow Ru^0 + xH_2O$$
$$La_2O_2CO_3 \leftrightarrow La_2O_3 + CO_2$$

In CO_2 rich streams, the re-oxidation of the active metal occurred:

$$Ru^0 + CO_2 \rightarrow RuO_x + CO$$

However, under DRM conditions for the two compositions tested, metallic Ru did not change its oxidation state and graphitic carbon and oxycarbonate formation was observed.

$$S - CH_4 \rightarrow S - C + 2H_2$$
$$La_2O_3 + CO_2 \leftrightarrow La_2O_2CO_3$$

The Ru1MV solid showed a higher reactivity of lanthanum oxycarbonate to the formation of La_2O_3 in a hydrogen flow even at low temperatures. In this solid, Ru was incorporated by wet impregnation leading to a higher Ru/La surface ratio. An explanation could be that the surface Ru species catalyzed type Ia oxycarbonate decomposition. However, these Ru species do not promote the gas-solid interaction that leads to oxycarbonate formation by reaction of the support with CO_2.

For the Ru1MV catalyst, the following phase transformation was also produced:

$$La_2O_2CO_3 \text{ type Ia} \rightarrow La_2O_2CO_3 \text{ type II}$$

When the Raman cell was fed with Ar, the formation of lanthanum oxide and the disappearance of carbonaceous deposits were observed in agreement with the reaction mechanism step:

$$La_2O_2CO_3 + C - S \rightarrow La_2O_3 + 2CO + S$$

Under CRM conditions, the same phase transformation occurred as in the case of DRM and also for the Ru2MV catalyst, the re-oxidation of Ru^0 species was observed:

$$Ru^0 + CO_2/O_2 \rightarrow RuO_x + CO/H_2O$$

This observation is in agreement with the low activity of this solid under CRM conditions. (Table 4). Finally, Fig. 12 summarizes the different cycles the solids were exposed to, all monitored by Raman spectroscopy. The conclusion of these thermal treatments was that the RuO_x could be re-reduced in the dry reforming of methane conditions for the Ru1MV catalyst. Moreover, in the Ru2MR catalyst, the re-oxidized Ru could be re-reduced even in CO_2 rich-atmospheres, such as CRM conditions.

4. Conclusions

All solids were active and stable for the dry and combined reforming of methane reactions. The catalysts synthesized with high surface lanthanum oxycarbonates were more active than the Ru/La_2O_3 solid previously studied [5].

In situ laser Raman studies allowed us to further our understanding of the solids transformations produced during the reaction and their influence on the activity and stability of the catalysts.

The Ru1MV catalyst with a higher Ru/La ratio was the solid that presented greater reactivity of oxycarbonates to La_2O_3, as the signal appeared at a lower reduction temperature (400 °C). In this sense, when this reduced solid was exposed to the reaction mixture, it showed a low reactivity of La_2O_3 for the oxycarbonate formation.

For the Ru2MV under CRM conditions, the Ru particles were partially re-oxidized. In addition, for the Ru1MV solid, the RuO_x species formed during the oxycarbonate decomposition could re-reduce under dry reforming of methane conditions. However, for the Ru2MR catalyst, the RuO_x species could be re-reduced even in oxidizing atmospheres, such as the CRM mixture.

Acknowledgments

The authors wish to acknowledge the financial support received from UNL, CONICET and ANPCyT. Thanks are also given to the Japan International Cooperation Agency (JICA) for the donation of the XRD, to ANPCyT for the purchase of the Raman instrument (PME 87-PAE 36985) and the UHV Multi Analysis System (PME 8–2003). Thanks are finally given to Elsa Grimaldi for the English language editing and to Fernanda Mori for the XPS measurements.

References

[1] Department of Energy Office of Fossil Energy and National Energy Technology Laboratory, Modern Shale Gas Development in the United States: A Primer, Department of Energy Office of Fossil Energy and National Energy Technology Laboratory, United States, 2009, pp. 1–116.
[2] B. Faroldi, E. Lombardo, L. Cornaglia, Appl. Catal., A 369 (2009) 15–26.
[3] H. Vidal, S. Bernal, R. Baker, G. Cifredo, D. Finol, J. Rodríquez-Izquierdo, Appl. Catal., A 208 (2001) 111–123.
[4] Z. Boukha, L. Fitian, M. López-Haro, M. Mora, J. Rafael Ruiz, C. Jiménez-Sanchidrián, G. Blanco, J.J. Calvino, G.A. Cifredo, S. Trasobares, S. Bernal, J. Catal. 272 (2010) 121–130.
[5] B. Faroldi, C. Carrara, E. Lombardo, L. Cornaglia, Appl. Catal., A 319 (2007) 38–46.
[6] R. Taylor, G. Schrader, Ind. Eng. Chem. Res. 30 (1991) 1016–1023.
[7] M. Scheithaeur, H. Knözinger, H. Vannice, J. Catal. 178 (1998) 701–705.
[8] B. Klingenberg, M.A. Vannice, Chem. Mater. 8 (1996) 2755–2768.
[9] R. Turcotte, J. Sawyer, L. Eyring, Inorg. Chem. 8 (1969) 238–246.
[10] V. Tsipouriari, X.E. Verykios, Catal. Today 64 (2001) 83–90.
[11] J. Múnera, S. Irusta, L. Cornaglia, E. Lombardo, D. Vargas Cesar, M. Schmal, J. Catal. 245 (2007) 25–34.
[12] C. Carrara, J. Múnera, E. Lombardo, L. Cornaglia, Top. Catal. 51 (2008) 98–106.
[13] B. Faroldi, M.L. Bosko, J. Múnera, E. Lombardo, L. Cornaglia, Catal. Today 213 (2013) 135–144.
[14] R. Cantrell, A. Ghenciu, K. Campbell, A. Minahan, M. Bhasin, A. Westwood, K. Nielsen, U.S. Patent 2002/0173420 A1, United States, 2002.
[15] L. Cornaglia, J. Múnera, S. Irusta, E. Lombardo, Appl. Catal., A 263 (2004) 91–101.
[16] S. Chan, A. Bell, J. Catal. 89 (1984) 433–441.
[17] H. Chan, C. Takoudis, M. Weaver, J. Catal. 172 (1997) 336–345.
[18] M. Mihaylov, E. Ivanova, Y. Hao, K. Hadjiivanov, H. Knozinger, B.C. Gates, J. Phys. Chem. C 112 (2008) 18973–18983.
[19] G. Yan, T. Wu, W. Weng, H. Toghiani, R. Toghiani, H. Wan, C. Pittman, J. Catal. 226 (2004) 247–259.
[20] J. Kehres, J.G. Jakobsen, J.W. Andreasen, J.B. Wagner, H. Liu, A. Molenbroek, J. Sehested, I. Chorkendorff, T. Vegge, J. Phys. Chem. C 116 (2012) 21407–21415.
[21] J.G. Jakobsen, T.L. Jørgensen, I. Chorkendorff, J. Sehested, Appl. Catal., A 377 (2010) 158–166.
[22] J.R. Rostrup-Nielsen, J-H. Bak Hansen, J. Catal. 144 (1993) 38–49.
[23] J. Wei, E. Iglesia, J. Phys. Chem. B 108 (13) (2004) 4094–4103.
[24] N. Matsui, K. Anzai, N. Akamatsu, K. Nakagawa, N. Ikenaga, T. Suzuki, Appl. Catal., A 179 (1999) 247–256.
[25] Y. Liu, F. Huang, J. Li, W. Weng, C. Luo, M. Wang, W. Xia, C. Huang, H. Wan, J. Catal. 256 (2008) 192–203.
[26] S. Lacombe, C. Geantet, C. Mirodatos, J. Catal. 151 (1994) 439–452.
[27] C. Klinke, R. Kurt, J. Bonard, K. Kern, J. Phys. Chem. B 106 (2002) 11191–11195.
[28] R. Escribano, J. Sloan, N. Siddique, N. Sze, T. Dudev, Vib. Spectrosc. 26 (2001) 179–186.
[29] L. Cornaglia, A. Gellman, J. Vac. Sci. Technol. 15 (1997) 2755–2765.
[30] F. Tuinstra, J. Koening, J. Chem. Phys. 53 (1970) 1126–1130.
[31] Y. Wang, D. Alsemeyer, R. Mc Creery, Chem. Mater. 2 (1990) 557.